MIT Libraries | DSpace@MIT

MIT Open Access Articles

Resolution Limits of Electron-Beam Lithography toward the Atomic Scale

The MIT Faculty has made this article openly available. ***Please share*** how this access benefits you. Your story matters.

Citation: Manfrinato, Vitor R., Lihua Zhang, Dong Su, Huigao Duan, Richard G. Hobbs, Eric A. Stach, and Karl K. Berggren. "Resolution Limits of Electron-Beam Lithography Toward the Atomic Scale." Nano Lett. (March 19, 2013): 130321102652000.

As Published: http://dx.doi.org/10.1021/nl304715p

Publisher: American Chemical Society (ACS)

Persistent URL: http://hdl.handle.net/1721.1/92829

Version: Author's final manuscript: final author's manuscript post peer review, without publisher's formatting or copy editing

Terms of Use: Article is made available in accordance with the publisher's policy and may be subject to US copyright law. Please refer to the publisher's site for terms of use.

Massachusetts Institute of Technology

Resolution limits of electron-beam lithography towards the atomic scale

Vitor R. Manfrinato[a], Lihua Zhang[b], Dong Su[b], Huigao Duan[c], Richard G. Hobbs[a], Eric A. Stach[b], and Karl K. Berggren[a,*]

[a] Electrical Engineering and Computer Science Department, Massachusetts Institute of Technology, 77 Massachusetts Avenue, Cambridge, Massachusetts 02139, USA;

[b] Center for Functional Nanomaterials, Brookhaven National Laboratory, Upton, New York 11973, USA;

[c] Micro–Nano Technologies Research Center, Hunan University, Changsha 410082, China

* Corresponding author: berggren@mit.edu

Abstract:

We investigated electron-beam lithography with an aberration-corrected scanning transmission electron microscope. We achieved 2 nm isolated feature size and 5 nm half-pitch in hydrogen silsesquioxane resist. We also analyzed the resolution limits of this technique by measuring the point-spread function at 200 keV. Furthermore, we measured the energy loss in the resist using electron-energy-loss spectroscopy.

Keywords: STEM lithography, electron beam lithography, high voltage electron beam lithography, hydrogen silsesquioxane, point spread function, EELS.

Electron-beam lithography (EBL) is widely used to achieve high resolution patterns[1-7] in nanotechnology research and development, but has been limited to 4 nm features[6, 8] and 8 nm half-pitch[6] (half of the periodicity of dense features) using conventional resists. A critical step to understand and thereby improve upon EBL resolution is quantifying the electron-beam deposited energy in the resist at the nanometer scale, i.e. the point-spread function (PSF). An accurate

measurement of the PSF is fundamental to measuring the overlap of deposited energy in the resist that limits pattern density (half-pitch) and gives rise to proximity effect.[9, 10] We measured the PSF at 200 keV from zero to 20 nm nm radii by combining an experimental method [11] and a calculation based on a sub-4-nm test structure. We also performed electron energy loss spectroscopy (EELS) to identify the pathways of energy loss in the resist.

Phenomena that limit EBL resolution include[5]: spot size, electron scattering, secondary-electron range, resist development, and mechanical stability of the resist. Many approaches have been used to investigate EBL resolution limits, addressing: electron-resist interactions,[2, 9, 11-13] resist processing,[14-16] and development. [17-19] In order to improve the resolution, STEM exposures at 100-350 kV acceleration voltages have been done to reduce resist-interaction volume (including the reduction of spot size). STEM lithography has also been done with conventional resists, such as poly(methyl methacrylate) (PMMA) [20] and calixarene [21], and in low-molecular-weight resists that are sublimated by electron-beam irradiation, such as NaCl.[3] The results on PMMA and calixarene showed 6 nm features and a 15 nm half-pitch. The results on NaCl showed ~2 nm features and 2 nm half-pitch, but with excessive exposure dose (~500 times higher than conventional resists). Electron-beam-induced deposition (EBID) is also capable of 2 nm feature size and 2 nm half-pitch,[22] but this technique is also 100 to 1000 times slower than EBL. Thus, a technique is needed that can achieve sub-5-nm-length-scale resolution at the dose level of conventional resists.

Here we show, with an aberration-corrected scanning transmission electron microscope (STEM), the fabrication of 2 nm isolated features and a 5-nm-half-pitch dot array using hydrogen silsesquioxane (HSQ) resist: to our knowledge, these are the highest resolution patterns of EBL achieved in conventional resists. We anticipate that this EBL technique would enable the

fabrication of novel plasmonic nanostructures,[23, 24] molecular devices,[25, 26] and bio-inspired functional materials.[27] We compared this technique with a 30 keV EBL system by measuring for the first time the PSF at 200 keV from zero to 20 nm radius, and calculating the resist energy-density contrast.

We investigated the resolution limits of EBL with a dedicated aberration-corrected STEM for a minimum spot size limitation (0.15 nm) and we used a 10-nm-thick SiN_x membrane as substrate for transmission electron microscopy (TEM) metrology (see details of exposure and metrology in SI). Thus, the EBL resolution was limited by the minimal forward scattering cross-section of 200 keV electrons, secondary-electron range, and resist development limitations at nanoscale.[6] The resist used was HSQ because it provides the highest resolution available.[4, 6] We used this system to determine the minimum realizable half-pitch and isolated lines with the smallest line width. These results gave us the practical resolution limits of the STEM as an EBL tool. Then, we measured the PSF to evaluate the fundamental resolution limit of the system. We used the measured PSF to calculate the energy-density contrast at 200 keV and compared with a 30 keV exposure.

Figure 1 shows the patterning capabilities of the STEM lithography technique. Figure 1a shows the schematics of the fabrication and metrology processes (see details in SI). After development, no apparent resist residues between the dots were found in the fabricated structures, as shown in Figure 1B and 1C. The 5-nm-half-pitch structure in Figure 1C represents a significant improvement over previous reports at 30 keV.[6] Challenges associated in fabricating these small features include resist collapse [28] and adhesion problems. Figure 1D shows an HSQ isolated line with the smallest width that did not collapse during development, which had average line width of 4 nm. To avoid resist collapse, we fabricated network-like structures (see

details and Figure S2 in SI). As shown in Figure 1E and 1F, 2 nm features were realized. We were also able to fabricate down to 1 nm features, but with poor uniformity (see details and Figure S3 in SI).

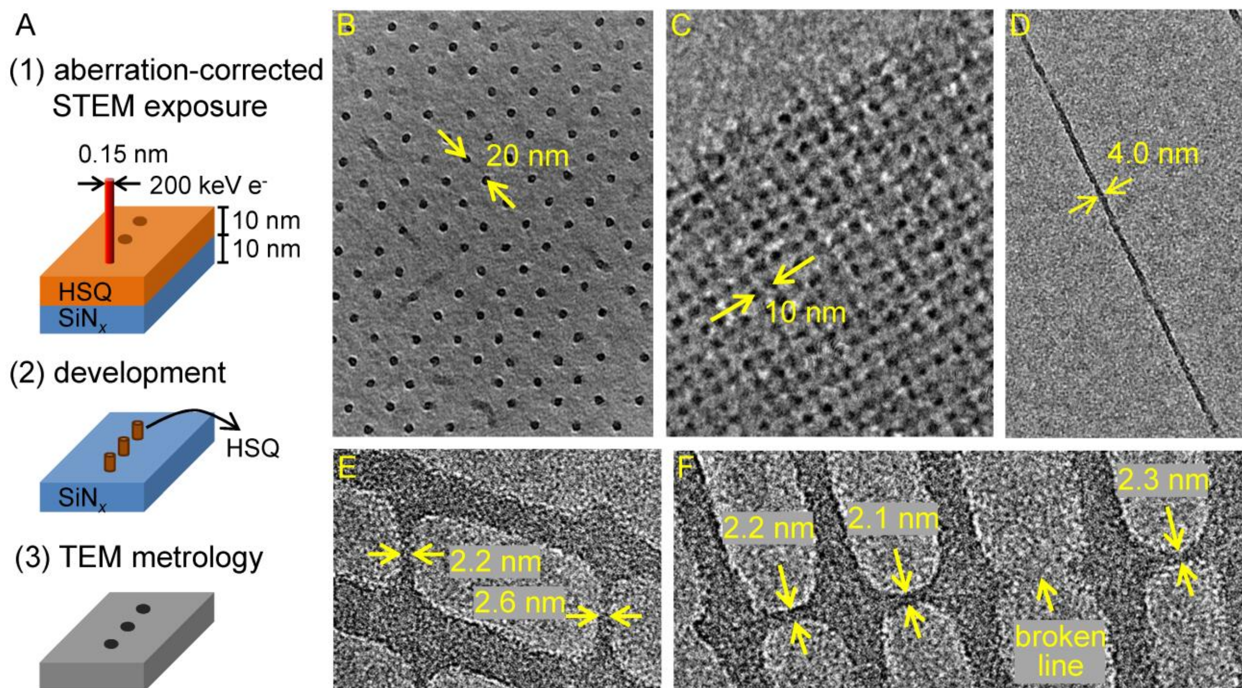

Figure 1. (A) Schematics of the STEM exposure, development, and TEM metrology. HSQ was spin-coated to be ~ 10 nm on a 10-nm-thick SiN_x membrane substrate, except on (C) where the SiN_x membrane was 50 nm thick. The exposure was at 200 keV with 0.5-2 nm step size. (B) 10-nm-half-pitch HSQ dot array with 5.1 ± 0.8 nm average feature diameter. (C) 5-nm-half-pitch HSQ dot array with 5.6 ± 1.2 nm average feature diameter. The dose was (B) 18 and (C) 6 fC/dot (108,000 and 36,000 electrons/dot). (D) shows an isolated feature with average line width of 4 ± 0.8 nm. The linear dose was 21 nC/cm (14,000 electrons/nm). The diameter and line width variation represent one standard deviation. (E) and (F) show the minimum feature size obtained by this method, with features as small as 2 nm with a linear dose of 8 nC/cm (5,300 electrons/nm).

These minimum features were only achieved by the combined use of sub-nanometer spot size, proper STEM stability, high-contrast development (contrast value, $\gamma = 10$), high-resolution (and sub-nanometer line-width roughness) capabilities of HSQ resist, and sub-nanometer

metrology obtained with TEM. In addition, the ultrathin SiN_x membrane should not affect the resolution compared to bulk substrates. The reason for this robustness is that the buildup of background energy density caused by backscattered electrons from a bulk substrate would only be significant for dense patterns with area on the order of the backscattered electron range (~10 µm), which is not the case in Figure 1.

We measured the dose for the patterns above (which is inversely proportional to pattern speed), in order to compare with other patterning methods. For instance, the dose to expose the 2 nm features (8 nC/cm) was 250 times smaller than used to expose NaCl resists,[3] and ~1000 times smaller than used for electron-beam-induced deposition.[22] From the reproducibility point of view, we measured the radii deviation between two distinct exposures with the same dose, i.e., dose latitude. The relative radii deviation was 13% (see details in SI).

Understanding the PSF is key for evaluating the resolution capabilities of EBL. To compare the resolution limit of this technique with others, we measured the PSF and used it to calculate the energy-density contrast (K) for a given pitch (p) (see calculation details in SI).

Figure 2A shows clearly that the PSF at 200 keV is sharper than that at 30 keV, indicating that 200 keV electrons have a significantly smaller short-range proximity effect (collaborative exposure from surrounding areas).

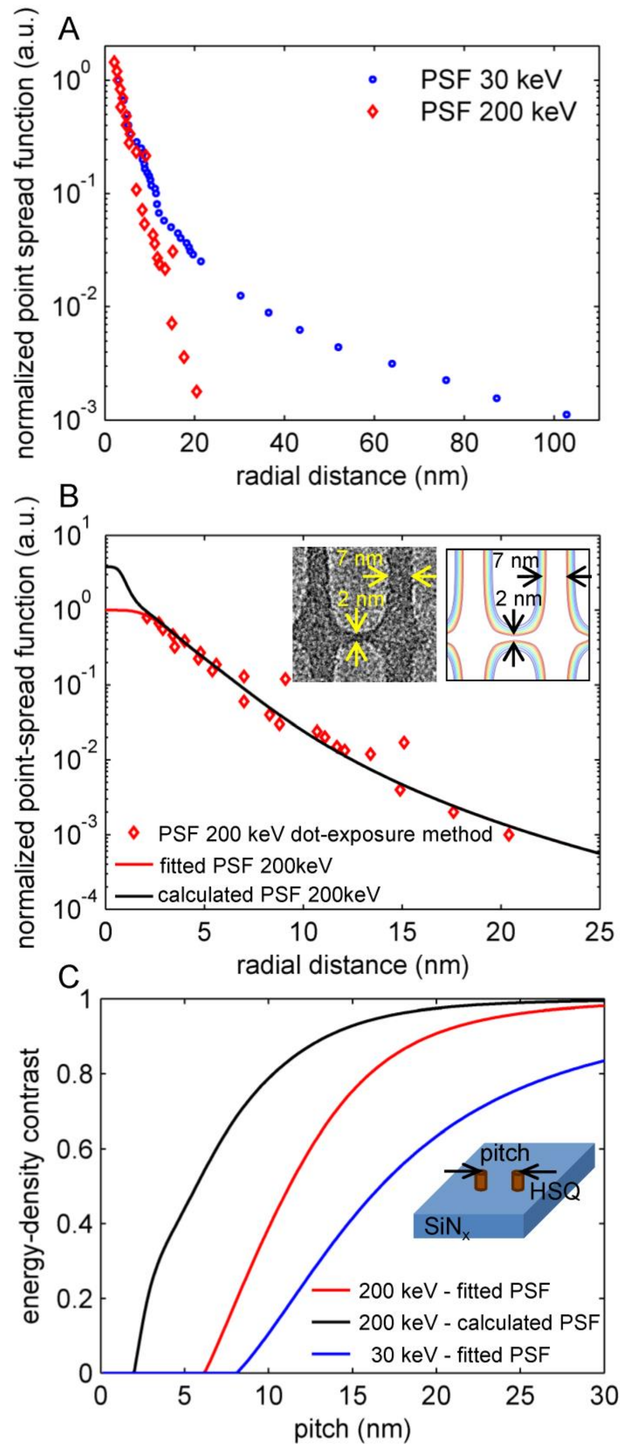

Figure 2. (A) The point-spread function (PSF) for ~10-nm-thick HSQ at 30 and 200 keV on SiN_x membrane substrate, showing that 200 keV electrons have a much narrower PSF compared to 30 keV. The PSF was measured by using single-pixel exposures[11] (see SI). (B) 200 keV PSF (red diamonds) and the fitting function (red curve). We iteratively calculated a PSF, named here as "calculated PSF", necessary to simulate the "H"-shaped test structure

shown in the leftmost inset (see details on SI). The rightmost inset shows the resultant energy density contours using this calculated PSF. Specifically; the red contour in this inset defines the simulated structure using the calculated PSF. The calculated PSF (black curve) had an extra bell-shaped function with a knee at 1 nm radius. (C) Calculated energy-density contrast, $K_{(p)} = \frac{E_{\max}-E_{\min}}{E_{\max}+E_{\min}}$, for the fabrication of two adjacent posts at 30 and 200 keV. The blue and red curves were calculated using the fitted PSF for 30 and 200 keV, respectively. The black curve was calculated using the calculated PSF from (B), predicting higher resolution than using the fitted PSF at 200 keV.

In the PSF measurement in Figure 2A, we were not able to achieve the fabrication of isolated posts with radius smaller than 2 nm. Then, we calculated a PSF fitting function that would simulate the "H"-shaped feature shown in the leftmost inset of Figure 2B to obtain the PSF for sub-2 nm radius. Based on a match of critical dimensions and radius of curvature between the "H"-shaped feature and the energy density contours in the rightmost inset of Figure 2B (see details in SI), we obtained what we named the "calculated PSF".

Figure 2C shows the consequence of having a narrow PSF on pattern density. The confined deposition of energy density translates into reduction of the short-range proximity effect, which was critical for achieving a higher resolution at 200 keV than at 30 keV (see calculation details in SI). Figure 2C also shows the importance of the PSF at sub-5-nm scale for estimating the resolution limit of an EBL system. For *K* of 0.5, we predict a resolution limit of 5 nm pitch for the 200 keV STEM system and 16 nm pitch for 30 keV EBL system in Ref 6.

Some challenges still remain to reaching sub-2-nm features and sub-5-nm half-pitch, such as feature collapse due to high-aspect-ratio features and capillary force during development, poor adhesion of the resist to the substrate, and mass-transport limitation during development.[6] Thus, a resist/development system that allowed patterns to be resolved with smaller *K,* should result in even higher resolution than 5 nm half-pitch being realized. In addition, we did not observe

isolated features smaller than 4 nm. One hypothesis is that HSQ may have a minimum stable volume after development. Therefore, linear structure may be more stable than isolated (or post) structures due to larger volume and smaller surface-to-volume ratio. However, further experiments need to be done to confirm this hypothesis.

The complexity of resist exposure, containing many energy loss processes, makes the direct measurement of the PSF a major challenge in beam-based lithography. For this reason, understanding the effects of secondary electrons in exposures have been limited to analytical[29] and Monte-Carlo models [12, 13, 30, 31]. To quantify the energy loss pathways in EBL, we directly measured the energy loss in HSQ using electron energy loss spectroscopy (EELS).

Figure 3 compares the low-loss EELS spectra in (red circles) 20-nm-thick HSQ on top of a 10-nm-thick SiN_x membrane and in (blue diamonds) a sample consisting only of a 10-nm-thick SiN_x membrane. We found that the sample with HSQ had 35% higher energy loss than the sample with only SiN_x. We analyzed HSQ and SiN_x samples with varying thicknesses to determine the proportion of energy loss only in HSQ. For the samples in Figure 3, we estimated that the energy loss in the HSQ was 42% of the total energy loss (see method in SI). We also observed in Figure 3 the bulk plasmon loss peak at 22.5 eV. This bulk plasmon peak is the largest energy loss component in HSQ. Generation of secondary electrons from plasmon decay [31-34] in the resist could be a significant route to resist exposure and may limit the resolution. However, further investigation would be necessary to validate this hypothesis.

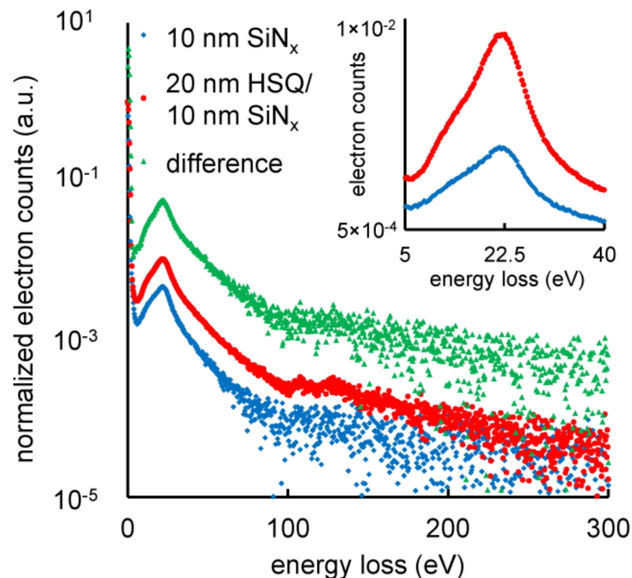

Figure 3. Electron energy loss spectra of 10-nm-thick SiN_x membrane (blue) and 20-nm-thick HSQ on top of 10-nm-thick SiN_x (red). The spectra were normalized by dividing the electron counts by its maximum value. The difference between these two spectra represents the energy loss in HSQ and is shown at the top (green – multiplied by ten for clarity), which represents ≈ 42% of the total energy loss. The bulk plasmon loss is the peak with highest intensity, at 22.5 eV. The inset shows a magnified view of the bulk plasmon loss peak.

In summary, we showed that 200 keV EBL with an aberration-corrected STEM is capable of patterning 2 nm isolated features and 5 nm half-pitch structures in HSQ, with significantly smaller dose than competing techniques such as EBID. We showed that 200 keV EBL exposures lead to higher contrast than 30 keV exposures. In addition, we determined the electron energy loss in HSQ at 200 keV.

Acknowledgements

We thank Jim Daley and Mark Mondol at the MIT Nanostructures Laboratory, Yong Zhang at the MRSEC Shared Experimental Facilities at MIT, and Aaron Stein at Brookhaven National Lab for

technical assistance. We would like to thank Joel K.W. Yang from IMRE A*Star at Singapore for insightful discussions. We thank Luca Grella, Mark McCord, and Alan Brodie from KLA-Tencor for insightful suggestions on electron energy loss spectroscopy for electron-beam lithography. In addition, we would like to thank the reviewers of this Letter for insightful discussions. This material is based upon work supported as part of the Center for Excitonics, an Energy Frontier Research Center funded by the U.S. Department of Energy, Office of Science, Office of Basic Energy Sciences under Award Number DE-SC0001088. The STEM lithography work was carried out at the Center for Functional Nanomaterials, Brookhaven National Laboratory, which is supported by the U.S. Department of Energy, Office of Basic Energy Sciences, under Contract No DE-AC02-98CH10886. This work made use of the MRSEC Shared Experimental Facilities at MIT, supported by the National Science Foundation under award number DMR-08-19762.

Supporting Information Available: Detailed description of experimental procedures and analysis. This material is available free of charge via the Internet at http://pubs.acs.org.

Table of Contents Graphic:

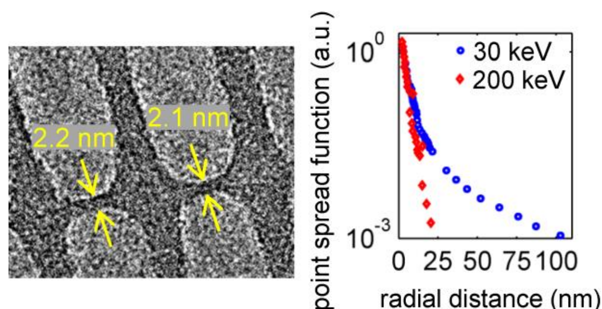

References

1. WELLS, O.; EVERHART, T.; MATTA, R. *Ieee Transactions on Electron Devices* **1965,** ED12, (10), 556-&.
2. BROERS, A.; MOLZEN, W.; CUOMO, J.; WITTELS, N. *Applied Physics Letters* **1976,** 29, (9), 596-598.
3. ISAACSON, M.; MURRAY, A. *Journal of Vacuum Science & Technology* **1981,** 19, (4), 1117-1120.
4. Yang, J.; Cord, B.; Duan, H.; Berggren, K.; Klingfus, J.; Nam, S.; Kim, K.; Rooks, M. *Journal of Vacuum Science & Technology B* **2009,** 27, (6), 2622-2627.
5. Cord, B.; Yang, J.; Duan, H.; Joy, D.; Klingfus, J.; Berggren, K. *Journal of Vacuum Science & Technology B* **2009,** 27, (6), 2616-2621.
6. Duan, H.; Manfrinato, V.; Yang, J.; Winston, D.; Cord, B.; Berggren, K. *Journal of Vacuum Science & Technology B* **2010,** 28, (6), C6H11-C6H17.
7. Pease, R. F. *J. Vac. Sci. Technol. B* **2010,** 28, (6), C6A1-C6A6.
8. Arjmandi, N.; Lagae, L.; Borghs, G. *Journal of Vacuum Science & Technology B* **2009,** 27, (4), 1915-1918.
9. HOWARD, R.; CRAIGHEAD, H.; JACKEL, L.; MANKIEWICH, P.; FELDMAN, M. *Journal of Vacuum Science & Technology B* **1983,** 1, (4), 1101-1104.
10. KYSER, D.; TING, C. *Journal of Vacuum Science & Technology* **1979,** 16, (6), 1759-1763.
11. RISHTON, S.; KERN, D. *Journal of Vacuum Science & Technology B* **1987,** 5, (1), 135-141.
12. KYSER, D.; VISWANATHAN, N. *Journal of Vacuum Science & Technology* **1975,** 12, (6), 1305-1308.
13. MURATA, K.; KYSER, D.; TING, C. *Journal of Applied Physics* **1981,** 52, (7), 4396-4405.
14. Olkhovets, A.; Craighead, H. *Journal of Vacuum Science & Technology B* **1999,** 17, (4), 1366-1370.
15. Namatsu, H.; Yamaguchi, T.; Nagase, M.; Yamazaki, K.; Kurihara, K. *Microelectronic Engineering* **1998,** 42, 331-334.
16. Fujita, J.; Ohnishi, Y.; Ochiai, Y.; Matsui, S. *Applied Physics Letters* **1996,** 68, (9), 1297-1299.
17. Hu, W.; Sarveswaran, K.; Lieberman, M.; Bernstein, G. *Journal of Vacuum Science & Technology B* **2004,** 22, (4), 1711-1716.
18. Yang, X.; Xiao, S.; Wu, W.; Xu, Y.; Mountfield, K.; Rottmayer, R.; Lee, K.; Kuo, D.; Weller, D. *Journal of Vacuum Science & Technology B* **2007,** 25, (6), 2202-2209.
19. Yang, J.; Berggren, K. *Journal of Vacuum Science & Technology B* **2007,** 25, (6), 2025-2029.
20. Vieu, C.; Carcenac, F.; Pepin, A.; Chen, Y.; Mejias, M.; Lebib, A.; Manin-Ferlazzo, L.; Couraud, L.; Launois, H. *Applied Surface Science* **2000,** 164, 111-117.
21. Yasin, S.; Hasko, D.; Carecenac, F. *Journal of Vacuum Science & Technology B* **2001,** 19, (1), 311-313.
22. van Dorp, W.; van Someren, B.; Hagen, C.; Kruit, P. *Nano Letters* **2005,** 5, (7), 1303-1307.
23. Ward, D.; Huser, F.; Pauly, F.; Cuevas, J.; Natelson, D. *Nature Nanotechnology* **2010,** 5, (10), 732-736.
24. Duan, H.; Fernandez-Dominguez, A.; Bosman, M.; Maier, S.; Yang, J. *Nano Letters* **2012,** 12, (3), 1683-1689.
25. Joachim, C.; Gimzewski, J.; Aviram, A. *Nature* **2000,** 408, (6812), 541-548.
26. Song, H.; Kim, Y.; Jang, Y.; Jeong, H.; Reed, M.; Lee, T. *Nature* **2009,** 462, (7276), 1039-1043.
27. Sarikaya, M.; Tamerler, C.; Jen, A.; Schulten, K.; Baneyx, F. *Nature Materials* **2003,** 2, (9), 577-585.
28. Duan, H.; Berggren, K. *Nano Letters* **2010,** 10, (9), 3710-3716.
29. Wu, B.; Neureuther, A. *Journal of Vacuum Science & Technology B* **2001,** 19, (6), 2508-2511.
30. JOY, D. *Microbeam Analysis* **1995,** 4, (3), 125-129.
31. LUO, S.; JOY, D. *Scanning Microscopy* **1990**, 127-146.
32. CHUNG, M.; EVERHART, T. *Physical Review B* **1977,** 15, (10), 4699-4715.

33. Werner, W.; Salvat-Pujol, F.; Smekal, W.; Khalid, R.; Aumayr, F.; Stori, H.; Ruocco, A.; Stefani, G. *Applied Physics Letters* **2011,** 99, (18).
34. Werner, W.; Ruocco, A.; Offi, F.; Iacobucci, S.; Smekal, W.; Winter, H.; Stefani, G. *Physical Review B* **2008,** 78, (23).